catalysts

MDPI

Article

A Trimetallic Pt_2NiCo/C Electrocatalyst with Enhanced Activity and Durability for Oxygen Reduction Reaction

Hilda M. Alfaro-López [1,2], Manuel A. Valdés-Madrigal [3,*], Hugo Rojas-Chávez [4], Heriberto Cruz-Martínez [5], Miguel A. Padilla-Islas [1], Miriam M. Tellez-Cruz [1,*] and Omar Solorza-Feria [1]

1 Departamento de Química, Cinvestav, Av. Instituto Politécnico Nacional 2508, San Pedro Zacatenco, Gustavo A. Madero, C.P. 07360, CDMX, Mexico; hilmar105@hotmail.com (H.M.A.-L.); adrianmapi@gmail.com (M.A.P.-I.); osolorza@cinvestav.mx (O.S.-F.)
2 Escuela Superior de Ingeniería Mecánica y Eléctrica—Departamento de Ingeniería Eléctrica—Edif. 2, Instituto Politécnico Nacional, U.P.A.L.M., Col. Lindavista, C.P. 07738, CDMX, Mexico
3 Instituto Tecnológico Superior de Ciudad Hidalgo. Av. Ing. Carlos Rojas Gutiérrez 2120, fracc. Valle de la herradura, Michoacán, C.P. 61100, Mexico
4 Tecnologico Nacional de Mexico, Instituto Tecnologico de Tlahuac II, Camino Real 625, Col. Jardines del Llano, San Juan Ixtayopan, C.P. 13508, CDMX, Mexico; huroch@gmail.com
5 Tecnologico de Monterrey, School of Engineering and Sciences, Atizapán de Zaragoza, Estado de México, C.P. 52926, Mexico; hcruzm@tec.mx
* Correspondence: mavm8405@hotmail.com (M.A.V.-M.); mtellez@cinvestav.mx (M.M.T.-C.)

Received: 10 December 2019; Accepted: 22 January 2020; Published: 2 February 2020



Abstract: Commercialization of the polymer electrolyte membrane fuel cell (PEMFC) requires that electrocatalysts for oxygen reduction reaction (ORR) satisfy two main considerations: materials must be highly active and show long-term stability in acid medium. Here, we describe the synthesis, physical characterization, and electrochemical evaluation of carbon-dispersed Pt_2NiCo nanocatalysts for ORR in acid medium. We synthesized a trimetallic electrocatalyst via chemical route in organic medium and investigated the physical properties of the Pt_2NiCo/C nanocatalyst by X-ray diffraction (XRD), energy-dispersive X-ray spectroscopy-scanning electron microscope (EDXS-SEM), and scanning transmission electron microscopy (STEM), whereas the catalytic activities of the Pt_2NiCo/C and Pt/C nanocatalysts were determined through cyclic voltammetry (CV), CO-stripping, and rotating disk electrode (RDE) electrochemical techniques. XRD and EDXS-SEM results confirmed the presence of the three metals in the nanoparticles, and scanning transmission electron microscopy (STEM) allowed observation of the Pt_2NiCo nanoparticles at ~10 nm. The measured specific activity for the synthesized nanocatalyst is ~6.4-fold higher than that of Pt/C alone, and its mass activity is ~2.2-fold higher than that of Pt/C, which is attributed to the synergistic interaction of the trimetallic electrocatalyst. Furthermore, the specific and mass activities of the synthesized material are maintained after the accelerated stability test, whereas the catalytic properties of Pt/C decreased. These results suggest that the Pt_2NiCo/C trimetallic nanocatalyst is a promising candidate cathode electrode for use in PEMFCs.

Keywords: trimetallic nanoparticles; mass activity; specific activity; stability

1. Introduction

The H_2-based polymer electrolyte membrane fuel cell (H_2-PEMFC) has increased in importance because of its high energy conversion efficiency and low emission of pollutants into the atmosphere. Additionally, H_2-PEMFCs can be designed according to diverse applications, including stationary,

portable, and automotive systems [1–3]. However, similar to other developing technologies, H_2-PEMFCs present challenges, including sluggish oxygen reduction reaction (ORR) kinetics that occur on the cathode side of a fuel cell. Therefore, there is a need to improve the performance of nanocatalysts to accelerate the cathodic reaction [4–6]. Current research efforts are focused on the design of electrode materials capable of enhancing kinetics and durability and reducing the cost associated with Pt-based cathode catalysts. In this context, noble-metal-based electrocatalysts and their alloys with low Pt content have been demonstrated to be an efficient and robust approach to address specific problems either in catalytic activity/selectivity or durability for the ORR, through understanding of the relationship between the electronic structure and catalytic activity of the catalyst [7,8]. For this reason, Pt-based bimetallic systems studied by different groups show that modifying size, morphology, and composition can promote superior activities and stabilities by the synthesized catalysts relative to those by commercially available Pt/C nanoparticles [9–12].

Another alternative showing increased relevance is the design of trimetallic catalysts based on their status as good candidates for the ORR in acid medium [13]. In this context, different trimetallic systems, such as $PtPdM_1$ [14], $PtIrM_1$ [15], $PtMoM_1$ [16], and PtM_1M_2 (where M_1 and M_2 are non-noble metals; e.g., Fe, Co, Ni, and Cu among others) have been studied as candidates for the ORR [17]. Among the investigated trimetallic systems, PtM_1M_2 systems have gained increased interest, because they allow the use of two non-noble metals; therefore, various PtM_1M_2 nanoparticles (e.g., PtNiCu, PtNiCo, and PtNiFe) for the ORR in acidic medium have been studied [17–20]. These PtM_1M_2 trimetallic systems exhibit outstanding catalytic activity for the ORR in an acid medium. However, the application of these systems as cathodes in H_2-PEMFCs needs to be studied extensively.

To contribute to research of trimetallic nanocatalysts for the ORR, we established a strategy for the design, synthesis, and characterization of a PtNiCo/C trimetallic electrocatalyst exhibiting enhanced activity and stability for the ORR in acid medium. It is important to note that some precedents serve as a starting point for this PtNiCo/C system. In this sense, several approaches have been reported. In 2010, Wanjala et al. [21] investigated the role of thermal treatment on the electrocatalytic properties of PtNiCo nanoparticles supported on carbon, finding that the mass activity (MA) of treated $Pt_{36}Ni_{15}Co_{49}$/C (800 °C and 926 °C) was approximately four-fold higher than that of commercial Pt/C. In a recent study, Arán-Ais et al. [22] reported that the electrocatalytic activity of shape-controlled octahedral PtNiCo nanoparticles showed a three-fold enhanced MA relative to commercial Pt/C and sustained high activity after 4000 voltammetry cycles. In 2016, Wang et al. [23] synthesized PtNiCo/C–N nanocomposites with controlled morphology, with these exhibiting catalytic activity and stability superior to that of Pt/C for the ORR. Recently, NiCoPt/C alloy nanoparticles were synthesized using a solvothermal process and evaluated for their electrochemical performance for the ORR in acid medium [24], demonstrating that the NiCoPt/C nanocatalyst presented a specific activity (SA) ~3.7-fold higher than that of Pt/C. Additionally, a recent theoretical and experimental study was performed on ordered Pt_2CoNi trimetallic electrocatalysts with an ORR catalytic activity five-fold to six-fold higher than that of Pt/C and showing excellent stability in acid medium [25]. In another study, a PtNiCo alloy nanocatalyst was obtained using a solvothermal process, followed by annealing and evaluated for the ORR in acidic medium, revealing that the PtNiCo-16h/C nanocatalyst showed an enhanced SA ~12-fold higher than that of commercial Pt/C and with excellent stability [26]. Furthermore, Pt-wrapped CoNi bimetallic nanoparticles were the subject of a theoretical study and experimental validation for ORR in acid medium [27,28], showing their superior catalytic activities relative to commercial Pt/C [28]. The catalytic activities and stabilities reported to the date motivated the present investigation of PtNiCo/C trimetallic systems for the ORR in H_2-PEMFCs.

In the present study, the synthesis, physical characterization, and electrochemical evaluation of the heat-treated Vulcan carbon dispersed Pt_2NiCo trimetallic nanocatalyst are investigated. The Pt_2NiCo catalyst was produced with a simple and low-cost chemical synthesis in organic medium, which has demonstrated to be a versatile method to produce PtNi/C bimetallic nanocatalysts with controlled size,

composition, and shape [29,30]. Hence, we have adjusted this protocol to synthesize the Pt_2NiCo/C trimetallic nanoparticles with enhanced electrocatalytic activity and stability for the ORR.

2. Results and Discussion

2.1. Physical Properties of the Pt_2NiCo/C Nanocatalyst

The powder XRD pattern of the as-synthesized Pt_2NiCo nanocatalyst is presented in Figure 1 after removing the background and compared with the Bragg reflections of Pt face-centered cubic (FCC; black marks), Ni FCC (red marks), and Co FCC (green marks). The diffraction peak positions of the trimetallic Pt_2NiCo nanoparticles show a shift to a higher 2θ as compared with metallic Pt, with the value for the Pt (111) peak in the reference located at 39.76°, whereas the experimental peak is at 40.47° (0.71° higher). Moreover, the peak positions of the Pt_2NiCo catalyst are located between elemental Pt, Ni, and Co. As previously reported, the significant shift to higher 2θ values relative to those of pure Pt is attributed to the formation of a Pt_2NiCo trimetallic system [25]. Because the Pt_2NiCo catalyst did not present superlattice peak positions similar to those reported by Lokanathan et al. [25], we inferred that the synthesized catalyst is not a face-centered tetragonal structure. Otherwise, the experimental findings obtained here are similar to those reported with an FCC structure [25,31]. The crystallite size was calculated using Topas Software [32] and considering an analysis of all the peaks of the diffractogram using a fundamental parameters approach for profile fitting. An average value for the crystallite size (11.25 nm) was obtained, with a weighted residual error of 5.917 and the goodness of fit at 2.17, thereby confirming a good fit of the model with the experimental data.

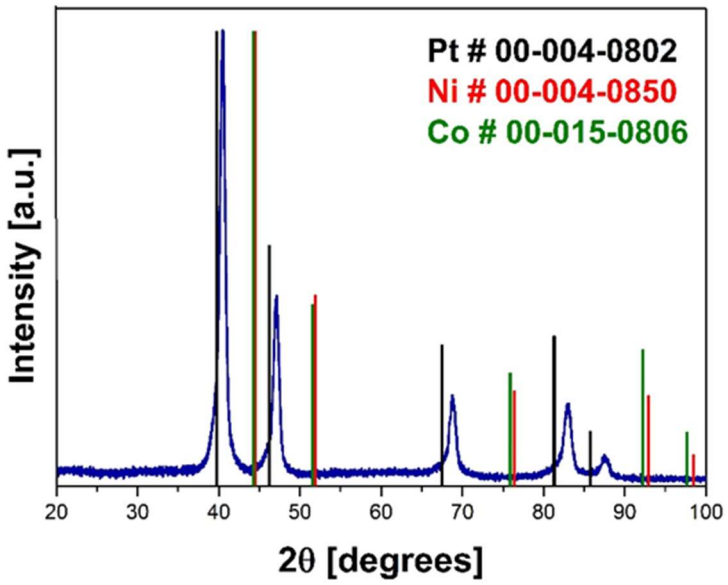


Figure 1. Powder diffraction pattern of the Pt_2NiCo/C nanocatalyst.

Before the dispersion of the Pt_2NiCo nanoparticles on the Vulcan carbon support, the morphological features of the prepared catalyst were investigated by STEM. Figure 2 shows that the Pt_2NiCo nanoparticles are agglomerated as depicted in the low-magnification STEM micrograph. However, it is noticeable that the Pt_2NiCo nanoparticles show a morphology of irregular quasi-spheres with an average size of ~9 to ~12 nm (Figure 2, inset).

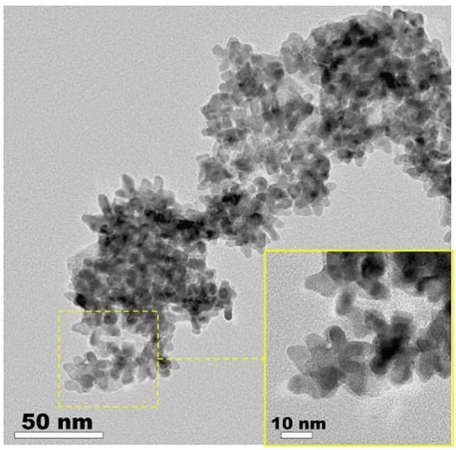


Figure 2. Low-magnification scanning transmission electron microscopy (STEM) micrograph of an agglomerate of Pt_2NiCo nanoparticles. The inset corresponds to a magnified view of the framed zone (dashed line).

Figure 3a displays a STEM micrograph of the Pt_2NiCo/C catalyst before the electrochemical measurements. In this figure, the inset displays a magnified view of the (continuous line) framed region depicting a quasi-spherical nanoparticle with a diameter of ~10 nm. Figure 3b, c show that the agglomerates comprised several nanoparticles with dimensions < 10 nm. Figure 3d shows the STEM image of the single Pt_2NiCo nanoparticle, revealing a rounded morphology and lattice fringes on its surface and d-spacing of 2.20 Å, which is agreed with the d-spacing (2.21 Å) reported for the (111) plane of Pt_2NiCo/C [25]. Additionally, comparing Figures 2 and 3, it is worth mentioning that the Vulcan carbon did not affect either the size or morphology of the Pt_2NiCo nanoparticles.

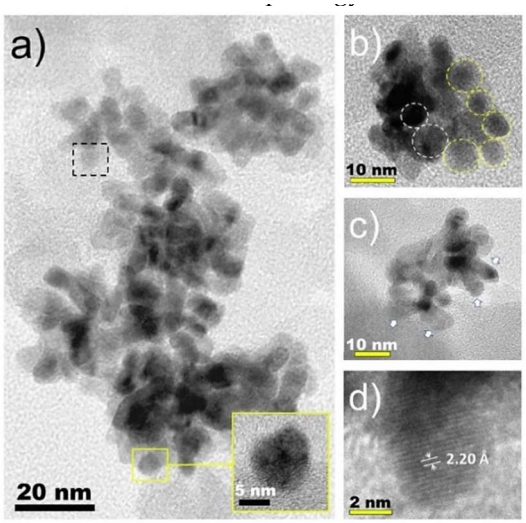


Figure 3. (**a**) STEM micrograph of the Pt_2NiCo/C nanocatalyst before the electrochemical measurements. (**b**,**c**) Agglomerates constituted by nanoparticles of the Pt_2NiCo/C catalyst. (**d**) Magnified view of the framed zone (dashed line) in (**a**).

Figure 4 shows a STEM image of the Pt_2NiCo/C catalyst after the accelerated stability test (5000 cycles of CV from 0.60 V to 1.0 V/RHE). As shown in Figure 4a, b, the isolated agglomerates are smaller relative to those formed before the electrochemical measurements. Although the nanoparticles formed linkages, these nanoparticles remained elongated, with rounded morphologies < 8 nm (Figure 4a–c). After the electrochemical measurements, the agglomerates presented cavities, with Figure 4d showing a magnified view of the framed zone in Figure 4c that provided further insight

into cavity distribution. The linkages among catalytic nanoparticles gave way to well-defined cavities, which are homogeneously distributed (Figure 4d). Therefore, this suggested that the occurrence of cavities in the agglomerates maintained the high activity of the Pt_2NiCo/C catalyst during the accelerated stability test.

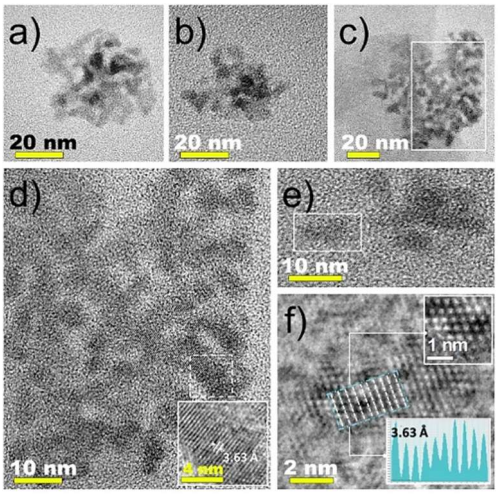


Figure 4. (**a**) STEM micrograph of the Pt_2NiCo/C catalyst after the accelerated stability test. (**b**,**c**) Agglomerates constituted by nanoparticles of the Pt_2NiCo/C catalyst. (**d**) Magnified view of the framed zone in (**c**). (**e**) The framed zone reveals the presence of an isolated, elongated and rounded nanoparticle, as well as the occurrence of a small agglomerate. (**f**) Magnified view of the framed zone in (**e**).

On the other hand, the lattice spacing computed from the high-resolution micrograph indicated that the d-spacing (3.63 Å) is consistent with that (3.66 Å) reported for the Pt_2NiCo/C (001) plane (Figure 4d, inset) [25,31]. Figure 4f shows a magnified view of the framed region in Figure 4e, with the lower inset showing that the (001) planes associated with Pt_2NiCo/C predominated, whereas the upper inset shows a zoomed image revealing bright and dark intensities. According to Lokanathan et al. [25], such intensities are associated with Pt and Co/Ni, respectively, because of the Z-contrast effect, which indicated the occurrence of Pt_2NiCo/C. In this context, the region of interest (Figure 4f, upper inset) was processed to obtain an atomic resolution image of the Pt_2NiCo/C. Analyzing this region, using the line profile tool in Gatan's Digital Micrograph software confirmed the d-spacing obtained (Figure 4f, lower inset).

To determine the chemical composition of the synthesized Pt_2NiCo/C nanocatalyst before and after the 5000 CV cycles, we performed EDXS-SEM. Such measurements unambiguously determined the chemical composition of the as-synthesized Pt_2NiCo/C nanocatalyst (Figure S1), with the average chemical composition of the as-synthesized Pt_2NiCo nanocatalyst at 56.1 ± 1.8 at.% Pt, 21.1 ± 1.2 at.% Ni, and 22.9 ± 0.7 at.% Co. In the as-synthesized Pt_2NiCo/C catalyst, we measured a metal loading of 20 wt.% (Pt_2NiCo) and a carbon loading of 80 wt.%. We used the EDXS-SEM results to normalize the Pt loading utilized in the electrochemical characterization. Additionally, EDSX-SEM detected the presence of ~2 to ~3% tungsten coming from $W(CO)_6$, which was used in Pt_2NiCo synthesis. Finally, a chemical composition of 65.7 at.% Pt, 30.2 at.% Ni, and 4.1 at.% Co was measured in the Pt_2NiCo nanoparticles after the 5000 CV cycles. It is observed a clear reduction of Co content in the Pt_2NiCo nanoparticles, which can be due to the dissolution of Co in acid medium during the 5000 CVs cycles.

2.2. Catalytic Activity for the ORR

We used the CV, CO-stripping, and RDE techniques to determine the electrocatalytic activity of the synthesized Pt_2NiCo/C and commercial Pt/C nanocatalysts. Figure 5a shows the CV profiles of

Pt_2NiCo/C and commercial Pt/C in a scanning potential window from 0.05 V/RHE to 1.05 V/RHE. It is worth noting that the CV profiles of the Pt_2NiCo/C and Pt/C materials differed (Figure 5a), and that three regions are identified in the CVs of both nanomaterials: (1) a hydrogen zone (0.05–0.3/RHE), (2) a double-layer capacitance (0.3–0.7 V/RHE), and (3) oxide and hydroxide adsorption (0.7–1.05 V/RHE). However, in the hydrogen zone, significant changes are observed between the Pt_2NiCo/C and Pt/C profiles. The Pt/C CV in the hydrogen adsorption/desorption zone showed a well-defined characteristic profile and high current density, whereas the synthesized nanocatalyst showed a large decrease in current density in this region. Previous studies suggest that the decrease in current could be associated with the presence of tungstate species (WO_3) formed and deposited during synthesis on the surface of Pt nanoparticles, which are expected to block the active sites [33].

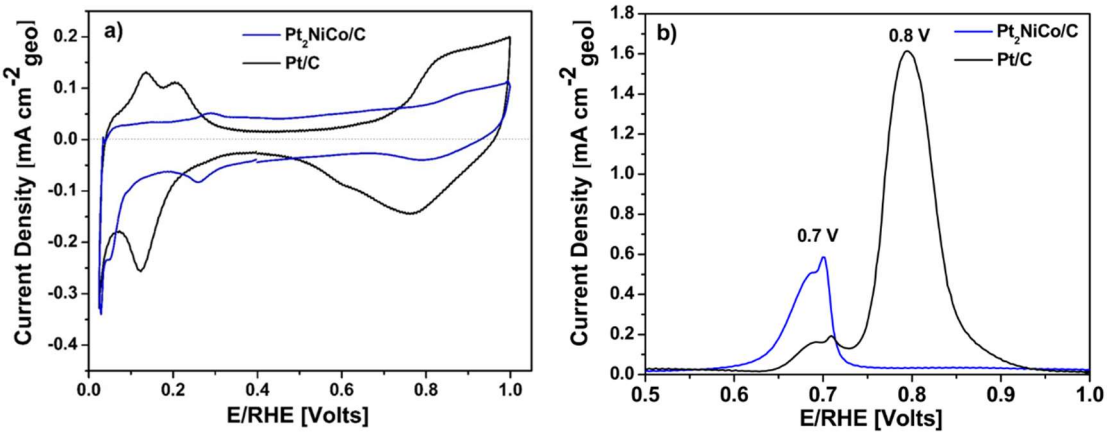


Figure 5. (**a**) Cyclic voltammograms of the Pt_2NiCo/C and Pt/C nanocatalysts measured at 20 mV s^{-1}. (**b**) CO electrooxidation peaks of Pt_2NiCo/C and Pt/C nanocatalysts with a scan rate of 20 mV s^{-1}.

To evaluate electrocatalytic activity toward the ORR, the measurement of the electrochemical active surface area (ECSA) of the nanocatalyst is of paramount importance, because it is used to determine the SA. The ECSAs of the synthesized Pt_2NiCo/C and commercial Pt/C nanocatalysts were obtained using the CO-stripping method. This technique is the most used for the ECSA determination on Pt-based nanocatalysts in ink-type electrodes and single-PEM fuel cells [34,35]. The ECSAs of the synthesized Pt_2NiCo/C and commercial Pt/C nanocatalysts were obtained using the following equation [36]:

$$\mathrm{ECSA}\left(\mathrm{m^2 g_{Pt}^{-1}}\right) = \left(\frac{\mathrm{Q_{CO}}}{420\ \mu\mathrm{C cm^{-2}} \times \mathrm{L_{Pt}}\left(\mathrm{mg_{Pt} cm^{-2}}\right) \times \mathrm{A_{geo}(cm^2)}}\right) \times 10^5 \quad (1)$$

where ECSA represents the Pt ECSA ($m^2 gPt^{-1}$), Q_{CO} is the charge transferred to oxidize the pre-adsorbed CO monolayer, 420 $\mu C cm^{-2}$ is used as a conversion factor, L_{Pt} is the Pt loading ($mg_{Pt} cm^{-2}$) on the working electrode, and A_{geo} (cm^2) is the geometric surface area of the glassy carbon electrode (i.e., 0.196 cm^2).

Figure 5b shows an illustration of the CO electrooxidation peaks of the Pt_2NiCo/C and commercial Pt/C nanocatalysts. Moreover, the nature of such a characteristic peak of the Pt_2NiCo/C (0.70 V/RHE) nanocatalyst differed from that of the Pt/C (0.8 V/RHE) nanocatalyst. This change in CO peak can be associated to the crystallographic planes, shape, size, composition, and agglomeration of the Pt_2NiCo nanoparticles [37,38]. The calculated ECSAs of the Pt_2NiCo/C and commercial Pt/C nanocatalysts are presented in Table 1, where it is observed that the Pt_2NiCo/C nanocatalyst presented a lower ECSA relative to that for Pt/C. This decrease can be attributed to the agglomeration of the Pt_2NiCo nanoparticles on the carbon (Figure 3).

We used the RDE technique to investigate the ORR of Pt_2NiCo/C and Pt/C in acid medium. The potentiodynamic polarization curves of the Pt_2NiCo/C and Pt/C electrocatalysts toward the ORR in acid medium are displayed in Figure 6. For the evaluated nanocatalysts, the three characteristic regions are identified, as previously reported [28,39]. The synthesized nanocatalyst presented a lower overpotential for ORR activation than that for Pt/C, and the half-wave potential ($E_{1/2}$) of Pt_2NiCo/C is 0.91 V/RHE, whereas that of Pt/C is 0.89 V/RHE. Based on the $E_{1/2}$ values, these results suggested that Pt_2NiCo/C is a better catalyst toward the ORR than Pt/C in acid medium.

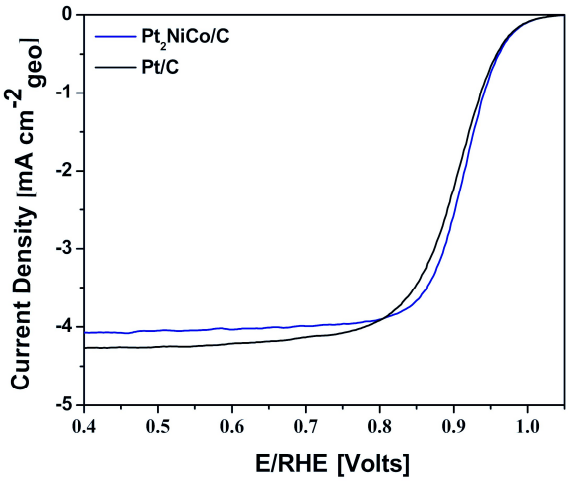


Figure 6. Potentiodynamic polarization curves of the Pt_2NiCo/C and Pt/C catalysts measured at 1600 rpm with a scan-rate of 20 mV s^{-1}.

Additionally, we used kinetic currents to determine the SA and MA. The protocol used for the mass transfer correction and determination of the SA and MA was previously reported [36]. The SA was calculated using the following equation:

$$SA\left(mAcm_{Pt}^{-2}\right) = \frac{I_k(A)}{\left(\frac{Q_{CO}(C)}{0.42mCcm_{Pt}^{-2}}\right)} \quad (2)$$

where I_k is the kinetic current.

Table 1 shows the kinetic parameters deduced from the electrochemical results of ORR on Pt_2NiCo/C and Pt/C in acid medium. The measured SA for the Pt_2NiCo/C nanocatalyst is ~6.4-fold higher than that of Pt/C, whereas the calculated MA of the Pt_2NiCo/C is ~2.2-fold higher than that of Pt/C. Additionally, these results are at least two-fold higher than those for the PtNi/C and PtCo/C electrocatalysts synthesized using a combination of mechanical milling and galvanic displacement and reported recently in our previous work [40]. Moreover, the MA results are similar to those reported by Wang et al. [20], where they used thermal annealing (600 °C) of PtNiCo/C nanoparticles to achieve an MA of 0.50 A mg^{-1}_{Pt}. However, in that study, the authors also reported a PtCoFe/C catalyst with an MA of 0.65 A mg^{-1}_{Pt} [20]. Furthermore, at low current density, the synthesized catalyst showed a Tafel slope of −56.2 mV dec^{-1}, which was similar to that for Pt/C (−55.5 mV dec^{-1}), assuming that the first electron transfer step ($O_2 + H^+ + e^- \rightarrow OOH$) on an active site is the rate-limiting step. From Kentucky–Levich plot for Pt_2NiCo/C, a B_0 value of 0.1153 mA cm^{-2} $rpm^{-1/2}$ was obtained, which agreed with the calculated value for the Pt/C catalyst (B_0 = 0.1380 mA cm^{-2} $rpm^{-1/2}$) and indicated a four-electron transfer process leading to water formation. These data suggested that the enhanced catalytic activity could be explained through interactions between Co and Ni with Pt on the carbon-supported catalyst.

Table 1. Kinetic parameters toward the oxygen reduction reaction (ORR) of the Pt_2NiCo/C and commercial Pt/C nanocatalysts in O_2-saturated 0.1 M $HClO_4$.

Catalyst	ECSA (m^2 g^{-1}_{Pt})	SA@0.9 V (mA cm^{-2}_{Pt})	MA@0.9 V (A mg^{-1}_{Pt})	$E_{1/2}$ (V)	Tafel slope (mV dec^{-1})	Bo (mA cm^{-2} $rpm^{-1/2}$)
Pt_2NiCo/C	29.88 ± 1.74	1.78 ± 0.11	0.53 ± 0.05	0.91	−56.2	0.1163
Pt/C	87.1	0.28	0.24	0.89	−55.5	0.1380

2.3. Catalytic Stability for the ORR

As previously discussed, the synthesized Pt_2NiCo/C catalyst can be considered a better candidate for ORR than the commercial Pt/C in acid medium; however, to better understand the electrocatalytic performance, we developed stability tests. To this end, the Pt_2NiCo/C and Pt/C nanocatalysts were subjected to a detailed stability test involving 5000 cycles of CV from 0.60 V to 1.0 V/RHE. The CO-stripping and RDE were used to determine the electrochemical performance after the 5000 cycles of CV. The CO electrooxidation peaks for the Pt_2NiCo/C (Figure 7a) and Pt/C nanocatalysts before and after stability testing did not change significantly. This suggested that the synthesized material maintained its ECSA, which can be attributed to the high stability of the supported trimetallic Pt_2NiCo nanoparticles, whereas results for the commercial Pt/C showed a loss of ~10% of its ECSA (Figure 8a). The initial potentiodynamic curves for synthesized Pt_2NiCo/C before and after 5000 potential cycles of CV are shown in Figure 7b. It is important to note that an outstanding result of this study is the high stability of the synthesized catalyst, given that there is no loss of activity after the 5000 cycles of CV. For Pt/C, the potentiodynamic curve shifted to higher overpotentials (Figure S2), suggesting that the Pt_2NiCo/C catalyst is more stable than Pt/C toward the ORR in acid medium. Figure 8 shows the average values of SA and MA for the Pt_2NiCo/C and Pt/C nanocatalysts, revealing increases in both for the Pt_2NiCo/C nanocatalyst after the 5000 CV cycles. This increase in catalytic activity can be associated with the cleaning (removal of the surfactant mixture) of the catalyst surface by application of the 5000 CV cycles to the Pt_2NiCo nanoparticles [41] and to the electronic structure modification of the Pt_2NiCo nanoparticles (Figure 4) [24,42]. The Pt/C nanocatalyst showed no significant change in SA after the 5000 CV cycles, whereas the MA decreased by ~20% (Figure 8c). Furthermore, the MA of the Pt_2NiCo/C nanoparticles after the 5000 CV cycles (0.57 A mg^{-1}_{Pt}) is similar to that reported previously for PtFeCo/C after 10,000 CV cycles (0.55A mg^{-1}_{Pt}) [20].

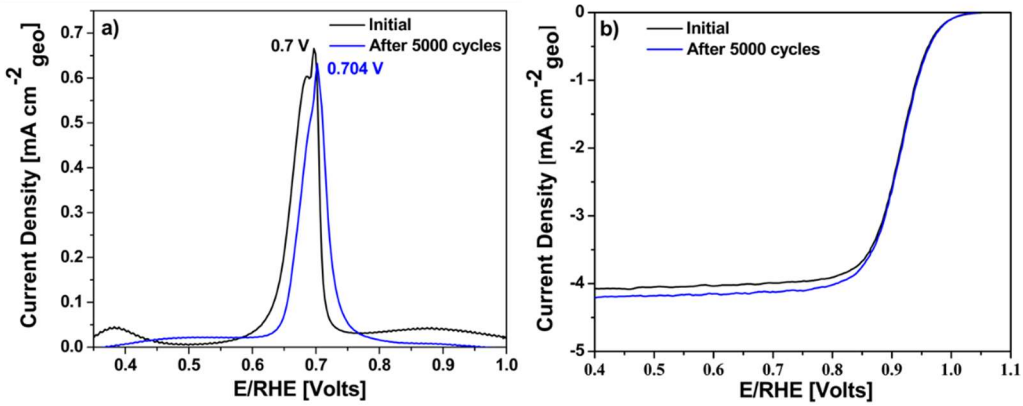


Figure 7. (**a**) CO electrooxidation peaks of Pt_2NiCo/C nanocatalyst initial and after the 5000 CVs with a scan-rate of 20 mV s^{-1}. (**b**) Potentiodynamic polarization curves of the Pt_2NiCo/C nanocatalyst initial and after the 5000 CVs measured at 1600 rpm with a scan rate of 20 mV s^{-1}.

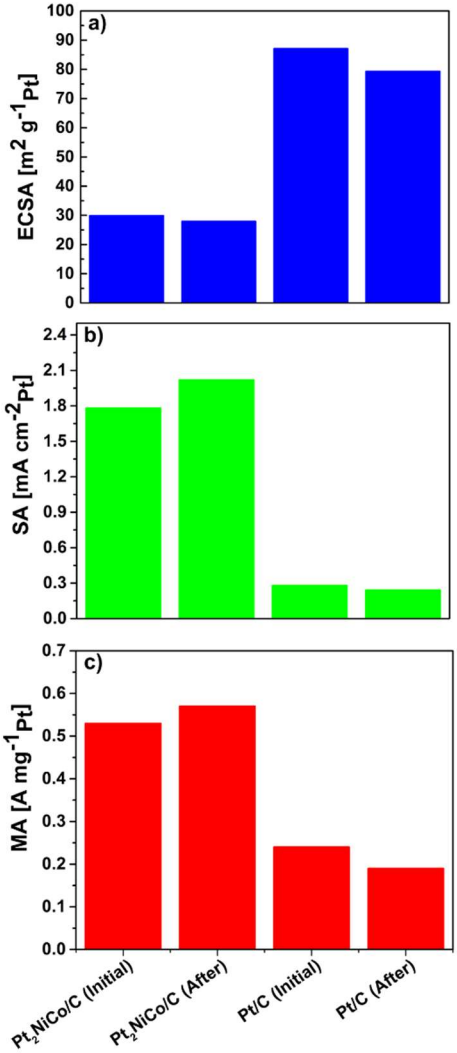


Figure 8. (**a**) electrochemical active surface area (ECSA), (**b**) specific activity (SA), and (**c**) mass activity (MA) of the Pt_2NiCo/C and Pt/C nanocatalysts initial and after the 5000 CV cycles.

3. Materials and Methods

3.1. Reagents

Nickel(II) acetylacetonate [$Ni(acac)_2$, 95%], platinum(II) acetylacetonate [$Pt(acac)_2$, 97%], dicobalt octacarbonyl [$Co_2(CO)_8$, >99.99%], tungsten hexacarbonyl [$W(CO)_6$, 97%], benzyl ether (BE, 98%), oleylamine (OAm, 70%), oleic acid (OA, 90%), perchloric acid ($HClO_4$, 70%), and hexane were acquired from Sigma-Aldrich, St. Louis, MO, USA. In all experiments, deionized water (18 MΩ/cm) was employed (Merck KGaA, Darmstadt, Hesse, Germany).

3.2. Synthesis of Pt_2NiCo Nanoparticles

For the synthesis of Pt_2NiCo nanoparticles, Pt $(acac)_2$ (0.1183 mmol, 46.6 mg) and Ni $(acac)_2$ (0.0443 mmol, 11.4 mg) were dissolved in OA (1.0 mL), OAm (2.0 mL), and BE (7.0 mL) in a three-neck flask, and the obtained solution was heated at 130 °C under magnetic stirring and nitrogen atmosphere. After nitrogen purging was stopped, $W(CO)_6$ (0.0276 mmol, 9.7 mg) and $Co_2(CO)_8$ (0.0146 mmol, 5 mg) were quickly added. In this study, $W(CO)_6$ was used as a reducing agent. The solution is then heated at 230 °C with heating rate of ~10 °C min^{-1} and maintained at 230 °C for 40 min. The

Pt_2NiCo nanoparticles were washed several times with hexane, and the supernatant was removed by centrifugation at 12,000 rpm for 5 min.

3.3. Preparation of the Pt_2NiCo/C Nanocatalyst

Pt_2NiCo nanoparticles were dispersed in 60 mL of isopropyl alcohol under magnetic stirring for 5 h. Simultaneously, the heat-treated Vulcan carbon was dispersed in isopropyl alcohol under agitation for 5 h. Thereafter, these two solutions were sonicated for 2 h to obtain a catalyst loading of 20 wt.% Pt_2NiCo dispersed on 80 wt.% Vulcan carbon. The Pt_2NiCo/C catalysts were then collected by centrifugation at 12,000 rpm for 10 min.

3.4. Physical Characterization

The Pt_2NiCo/C nanocatalyst was characterized through powder X-ray diffraction (XRD), scanning transmission electron microscopy (STEM), and energy-dispersive X-ray spectroscopy (EDXS). XRD was used to obtain the diffraction pattern of the Pt_2NiCo/C nanocatalyst, with the XRD measurements developed in a Bruker (BRUKER AXS, Inc., MA, USA) diffractometer with Cu Kα radiation (λ = 1.54 Å). The PDF-2 database was used for pattern identification. The average elemental composition of the Pt_2NiCo/C nanoparticles was determined using an EDXS system coupled to a Zeiss Auriga scanning electron microscope (SEM; Carl Zeiss, Oberkochen, Germany) operated at 20 kV. The shape and size of the Pt_2NiCo/C trimetallic nanoparticles were determined using an ARM200F-JEOL microscope (JEOL, Tokyo, Japan) operated at 200 keV. All STEM data were analyzed using the commercial software Digital Micrograph (Gatan Inc., Pleasanton, CA, USA).

3.5. Electrochemical Measurements

Catalytic inks were fabricated for the Pt_2NiCo/C and Pt/C (Pt/C Etek® 20 wt.%) catalysts according to a previously reported protocol [43] and deposited on a glassy carbon disk electrode (0.196 cm^2) with Pt loadings of 20 ± 2 $\mu g_{Pt} cm_{geo}^{-2}$. Electrochemical experiments were performed at room temperature (25 ± 2 °C) in a three-electrode electrochemical cell using a 0.1 M $HClO_4$ solution as electrolyte. An Autolab PGSTAT302N potentiostat/galvanostat (Metrohm Autolab B.V., Utrecht, Utrecht, The Netherlands) was used for the electrochemical procedures. A platinum mesh and a reversible hydrogen electrode (RHE) were employed as the counter electrode and reference electrode, respectively. The catalytic activities of Pt_2NiCo/C and Pt/C were investigated using cyclic voltammetry (CV), CO-stripping, and a rotating disk electrode (RDE). The description of these procedures was reported previously [39].

4. Conclusions

Here, we investigated a trimetallic Pt_2NiCo/C nanocatalyst with enhanced activity and durability toward the ORR in acid medium. The chemical synthesis with OAm, OA, BE, and $W(CO)_6$ (reducing agent) was demonstrated to be a versatile protocol for producing trimetallic nanoparticles (~10 nm). XRD, EDXS-SEM, and STEM analyses confirmed the co-existence of the three metals in the synthesized Pt_2NiCo nanoparticles, and the computed SA for the Pt_2NiCo/C nanocatalyst is ~6.4-fold higher relative to that for Pt/C, whereas the calculated MA for Pt_2NiCo/C is ~2.2-fold higher than that of Pt/C. Additionally, the SA and MA of the synthesized material is maintained after accelerated stability testing, whereas for Pt/C, these properties decreased. These results suggest that the Pt_2NiCo/C trimetallic nanocatalyst is a better candidate than Pt/C toward the ORR in acid medium. Furthermore, the Pt_2NiCo/C catalyst fulfilled the expectations required for a better catalyst, including decreased Pt content in the chemical composition, increased catalytic activity, and promising long-term stability for ORR.

Supplementary Materials: The following are available online at http://www.mdpi.com/2073-4344/10/2/170/s1, Figure S1: (**a**) a presentative SEM image of the region analyzed. (**b**) image of Co, Ni, Pt and C overlap, (**c**), (**d**), (**e**)

(**f**) are distributions of Co, Ni, Pt, and C atoms, respectively. Figure S2: Polarization curves of the Pt/C nanocatalyst initial and after 5000 CVs obtained at 1600 rpm with a scan rate of 20 mV s^{-1}.

Author Contributions: Conceptualization, H.M.A.-L., H.C.-M., M.M.T.-C. and O.S.-F.; Formal analysis, H.M.A.-L., M.A.V.-M., H.R.-C., H.C.-M., M.A.P.-I. and M.M.T.-C.; Investigation, H.M.A.-L., H.R.-C. and M.A.P.-I.; Writing—original draft, H.M.A.-L., M.A.V.-M., H.C.-M., M.A.P.-I. and O.S.-F.; Writing—review & editing, H.M.A.-L., M.A.V.-M., H.R.-C., M.M.T.-C. and O.S.-F. All authors have read and agreed to the published version of the manuscript

Funding: This research was funded by CONACYT-SENER, grant number 245920 and SEP-CINVESTAV, grant number 15.

Acknowledgments: H. M. Alfaro-López acknowledges CINVESTAV for the postdoctoral position and, COTEBAL for her postdoctoral scholarship. H. Cruz-Martínez and M. M. Tellez-Cruz thank CONACYT for their doctoral scholarships. M. A. Leyva-Ramírez is recognized by the XRD analysis. We thank to Angel Guillen-Cervantes and Jorge Roque by the EDXS-SEM measurements.

Conflicts of Interest: The authors declare no conflict of interest.

References

1. Brouzgou, A.; Song, S.Q.; Tsiakaras, P. Low and non-platinum electrocatalysts for PEMFCs: Current status, challenges and prospects. *Appl. Catal. B* **2012**, *127*, 371–388. [CrossRef]
2. Sharaf, O.Z.; Orhan, M.F. An overview of fuel cell technology: Fundamentals and applications. *Renew. Sust. Energ. Rev.* **2014**, *32*, 810–853. [CrossRef]
3. Wang, Y.; Chen, K.S.; Mishler, J.; Cho, S.C.; Adroher, X.C. A review of polymer electrolyte membrane fuel cells: Technology, applications, and needs on fundamental research. *Appl. Energ.* **2011**, *88*, 981–1007. [CrossRef]
4. Cruz-Martínez, H.; Tellez-Cruz, M.M.; Guerrero-Gutiérrez, O.X.; Ramírez-Herrera, C.A.; Salinas-Juárez, M.G.; Velázquez-Osorio, A.; Solorza-Feria, O. Mexican contributions for the improvement of electrocatalytic properties for the oxygen reduction reaction in PEM fuel cells. *Int. J. Hydrogen Energy* **2019**, *44*, 477–491. [CrossRef]
5. Debe, M.K. Electrocatalyst approaches and challenges for automotive fuel cells. *Nature* **2012**, *486*, 43–51. [CrossRef]
6. Jacob, T. The mechanism of forming H_2O from H_2 and O_2 over a Pt catalyst via direct oxygen reduction. *Fuel Cells* **2006**, *6*, 159–181. [CrossRef]
7. Yin, H.-J.; Zhou, J.-H.; Zhang, Y.-W. Shaping well-defined noble-metal-based nanostructures for fabricating high-performance electrocatalysts: Advances and perspectives. *Inorg. Chem. Front.* **2019**, *6*, 2582–2618. [CrossRef]
8. Huang, S.; Shan, A.; Wang, R. Low Pt alloyed nanostructures for fuel cells catalysts. *Catalysts* **2018**, *8*, 538. [CrossRef]
9. Wu, J.; Yang, H. Platinum-based oxygen reduction electrocatalysts. *Acc. Chem. Res.* **2013**, *46*, 1848–1857. [CrossRef]
10. Shao, M.; Chang, Q.; Dodelet, J.P.; Chenitz, R. Recent advances in electrocatalysts for oxygen reduction reaction. *Chem. Rev.* **2016**, *116*, 3594–3657. [CrossRef]
11. Yang, T.; Pukazhselvan, D.; Da Silva, E.L.; Santos, M.C.; Meng, L.; Ramasamy, D.; Jothi, S.; Graça, V.; Shi, S. Highly branched PtCu nanodandelion with high activity for oxygen reduction reaction. *Int. J. Hydrogen Energy* **2019**, *44*, 174–179. [CrossRef]
12. Bing, Y.; Liu, H.; Zhang, L.; Ghosh, D.; Zhang, J. Nanostructured Pt-alloy electrocatalysts for PEM fuel cell oxygen reduction reaction. *Chem. Soc. Rev.* **2010**, *39*, 2184–2202. [CrossRef] [PubMed]
13. Guo, S.; Zhang, X.; Zhu, W.; He, K.; Su, D.; Mendoza-Garcia, A.; Ho, S.F.; Lu, G.; Sun, S. Nanocatalyst superior to Pt for oxygen reduction reactions: The case of core/shell Ag(Au)/CuPd nanoparticles. *J. Am. Chem. Soc.* **2014**, *136*, 15026–15033. [CrossRef] [PubMed]
14. Cruz-Martínez, H.; Tellez-Cruz, M.M.; Rojas-Chávez, H.; Ramírez-Herrera, C.A.; Calaminici, P.; Solorza-Feria, O. NiPdPt trimetallic nanoparticles as efficient electrocatalysts towards the oxygen reduction reaction. *Int. J. Hydrogen Energy* **2019**, *44*, 12463–12469. [CrossRef]
15. Loukrakpam, R.; Wanjala, B.N.; Yin, J.; Fang, B.; Luo, J.; Shao, M.; Protsailo, L.; Kawamura, T.; Chen, Y.; Petkov, V.; et al. Structural and electrocatalytic properties of PtIrCo/C catalysts for oxygen reduction reaction. *ACS Catal.* **2011**, *1*, 562–572. [CrossRef]

16. Jia, Q.; Zhao, Z.; Cao, L.; Li, J.; Ghoshal, S.; Davies, V.; Stavitski, Y.E.; Attenkofer, K.; Liu, Z.; Li, M.; et al. Roles of Mo surface dopants in enhancing the ORR performance of octahedral PtNi nanoparticles. *Nano Lett.* **2018**, *18*, 798–804. [CrossRef]
17. Antolini, E. The oxygen reduction on Pt-Ni and Pt-Ni-M catalysts for low-temperature acidic fuel cells: A review. *Int. J. Energ Res.* **2018**, *42*, 3747–3769. [CrossRef]
18. Chou, S.W.; Shyue, J.J.; Chien, C.H.; Chen, C.C.; Chen, Y.Y.; Chou, P.T. Surfactant-directed synthesis of ternary nanostructures: Nanocubes, polyhedrons, octahedrons, and nanowires of PtNiFe. Their shape-dependent oxygen reduction activity. *Chem. Mater.* **2012**, *24*, 2527–2533. [CrossRef]
19. Nguyen, M.T.; Wakabayashi, R.H.; Yang, M.; Abruña, H.D.; DiSalvo, F.J. Synthesis of carbon supported ordered tetragonal pseudo-ternary Pt2M'M" (M= Fe, Co, Ni) nanoparticles and their activity for oxygen reduction reaction. *J. Power Sources* **2015**, *280*, 459–466. [CrossRef]
20. Wang, Z.; Yao, X.; Kang, Y.; Xia, D.; Gan, L. Rational development of structurally ordered platinum ternary intermetallic electrocatalysts for oxygen reduction reaction. *Catalysts* **2019**, *9*, 569. [CrossRef]
21. Wanjala, B.N.; Loukrakpam, R.; Luo, J.; Njoki, P.N.; Mott, D.; Zhong, C.J.; Shao, M.; Protsailo, L.; Kawamura, T. Thermal treatment of PtNiCo electrocatalysts: Effects of nanoscale strain and structure on the activity and stability for the oxygen reduction reaction. *J. Phys. Chem. C* **2010**, *114*, 17580–17590. [CrossRef]
22. Arán-Ais, R.M.; Dionigi, F.; Merzdorf, T.; Gocyla, M.; Heggen, M.; Dunin-Borkowski, R.E.; Gliech, M.; Solla-Gullón, J.; Herrero, E.; Feliu, J.M.; et al. Elemental anisotropic growth and atomic-scale structure of shape-controlled octahedral Pt-Ni-Co alloy nanocatalysts. *Nano Lett.* **2015**, *15*, 7473–7480. [CrossRef] [PubMed]
23. Wang, Q.; Zhao, Q.; Su, Y.; Zhang, G.; Xu, G.; Li, Y.; Liu, B.; Zheng, D.; Zhang, J. Hierarchical carbon and nitrogen adsorbed PtNiCo nanocomposites with multiple active sites for oxygen reduction and methanol oxidation reactions. *J. Mat. Chem. A* **2016**, *4*, 12296–12307. [CrossRef]
24. Lokanathan, M.; Patil, I.M.; Usman, A.K.; Swami, A.; Walke, P.; Navaneethan, M.; Kakade, B. Unusual enhancement in the electroreduction of oxygen by NiCoPt by surface tunability through potential cycling. *RSC Adv.* **2017**, *7*, 11777–11785. [CrossRef]
25. Lokanathan, M.; Patil, I.M.; Navaneethan, M.; Parey, V.; Thapa, R.; Kakade, B. Designing of stable and highly efficient ordered Pt_2CoNi ternary alloy electrocatalyst: The origin of dioxygen reduction activity. *Nano Energy* **2018**, *43*, 219–227. [CrossRef]
26. Lokanathan, M.; Patil, I.M.; Kakade, B. Trimetallic PtNiCo nanoflowers as efficient electrocatalysts towards oxygen reduction reaction. *Int. J. Hydrogen Energy* **2018**, *43*, 8983–8990. [CrossRef]
27. Flores-Rojas, E.; Cruz-Martínez, H.; Tellez-Cruz, M.M.; Pérez-Robles, J.F.; Leyva-Ramírez, M.A.; Calaminici, P.; Solorza-Feria, O. Electrocatalysis of oxygen reduction on CoNi-decorated-Pt nanoparticles: A theoretical and experimental study. *Int. J. Hydrogen Energy* **2016**, *41*, 23301–23311. [CrossRef]
28. Flores-Rojas, E.; Cruz-Martínez, H.; Rojas-Chávez, H.; Tellez-Cruz, M.M.; Reyes-Rodríguez, J.L.; Cabañas-Moreno, J.G.; Calaminici, P.; Solorza-Feria, O. A combined DFT and experimental investigation of Pt-wrapped CoNi nanoparticles for the oxygen reduction reaction. *Electrocatalysis* **2018**, *9*, 662–672. [CrossRef]
29. Choi, S.I.; Xie, S.; Shao, M.; Odell, J.H.; Lu, N.; Peng, H.C.; Protsailo, L.; Guerrero, S.; Park, J.; Xia, X.; et al. Synthesis and characterization of 9 nm Pt–Ni octahedra with a record high activity of 3.3 A/mgPt for the oxygen reduction reaction. *Nano Lett.* **2013**, *13*, 3420–3425. [CrossRef]
30. Choi, S.I.; Xie, S.; Shao, M.; Lu, N.; Guerrero, S.; Odell, J.H.; Park, J.; Wang, J.; Kim, M.J.; Xia, Y. Controlling the size and composition of nanosized Pt-Ni octahedra to optimize their catalytic activities toward the oxygen reduction reaction. *ChemSusChem* **2014**, *7*, 1476–1483. [CrossRef]
31. Chen, L.; Zhu, J.; Xuan, C.; Xiao, W.; Xia, K.; Xia, W.; Lai, C.; Xin, H.L.; Wang, D. Effects of crystal phase and composition on structurally ordered Pt-Co-Ni/C ternary intermetallic electrocatalysts for the formic acid oxidation reaction. *J. Mat. Chem. A* **2018**, *6*, 5848–5855. [CrossRef]
32. Bruker AXS. *TOPAS V3: General Profile and Structure Analysis Software for Powder Diffraction Data*; User manual; Bruker AXS: Karlsruhe, Germany, 2005.
33. Bott-Neto, J.L.; Ticianelli, E.A. Activity and Electrochemical Stability of Pt-and Pt_2Ni-α-WC/C Catalysts for the Oxygen Reduction Reaction in Acid Media. *ChemElectroChem* **2018**, *5*, 1364–1372. [CrossRef]

34. Lindström, R.W.; Kortsdottir, K.; Wesselmark, M.; Oyarce, A.; Lagergren, C.; Lindbergh, G. Active Area Determination of Porous Pt Electyrodes Used Polymer Electrolyte Fuel Cells: Temperature and Humidity Effects. *J. Electrochem. Soc.* **2010**, *157*, B1795–B1801. [CrossRef]
35. Brightman, E.; Hinds, G.; O'Malley, R. In situ measurement of active catalyst surface area in fuel cell stacks. *J. Power Sources* **2013**, *242*, 244–254. [CrossRef]
36. Garsany, Y.; Baturina, O.A.; Swider-Lyons, K.E.; Kocha, S.S. Experimental methods for quantifying the activity of platinum electrocatalysts for the oxygen reduction reaction. *Anal. Chem.* **2010**, *82*, 6321–6328. [CrossRef]
37. Maillard, F.; Schreier, S.; Hanzlik, M.; Savinova, E.R.; Weinkauf, S.; Stimminga, U. Influence of particle agglomeration on the catalytic activity of carbon-supported Pt nanoparticles in CO monolayer oxidation. *Phys. Chem. Chem. Phys.* **2005**, *7*, 385–393. [CrossRef]
38. Ciapina, E.G.; Santos, S.F.; Gonzalez, E.R. Electrochemical CO stripping on nanosized Pt surfaces in acid media: A review on the issue of peak multiplicity. *J. Electroanal. Chem.* **2018**, *815*, 47–60. [CrossRef]
39. Tellez-Cruz, M.M.; Padilla-Islas, M.A.; Godínez-Salomón, J.F.; Lartundo-Rojas, L.; Solorza-Feria, O. Y-OH-decorated-Pt/C electrocatalyst for oxygen reduction reaction. *Int. J. Hydrogen Energy* **2016**, *41*, 23318–23328. [CrossRef]
40. Flores-Rojas, E.; Reyes-Rodríguez, J.L.; Cruz-Martínez, H.; Rojas-Chávez, H.; Samaniego-Benítez, J.E.; Solorza-Feria, O. Applications of cathodic $Co_{100-X}Ni_X$ (x = 0, 30, 70, and 100) electrocatalysts chemically coated with Pt for PEM fuel cells. *Int. J. Hydrogen Energy* **2020**. [CrossRef]
41. Solla-Gullón, J.; Montiel, V.; Aldaz, A.; Clavilier, J. Electrochemical characterisation of platinum nanoparticles prepared by microemulsion: How to clean them without loss of crystalline surface structure. *J. Electroanal. Chem.* **2000**, *491*, 69–77. [CrossRef]
42. Wang, D.; Yu, Y.; Xin, H.L.; Hovden, R.; Ercius, P.; Mundy, J.A.; Chen, H.; Richard, J.H.; Muller, D.A.; DiSalvo, F.J.; et al. Tuning oxygen reduction reaction activity via controllable dealloying: A model study of ordered Cu_3Pt/C intermetallic nanocatalysts. *Nano Lett.* **2012**, *12*, 5230–5238. [CrossRef] [PubMed]
43. Kocha, S.S.; Shinozaki, K.; Zack, J.W.; Myers, D.J.; Kariuki, N.N.; Nowicki, T.; Stamenkovic, V.; Kang, Y.; Li, D.; Papageorgopoulos, D. Best practices and testing protocols for benchmarking ORR activities of fuel cell electrocatalysts using rotating disk electrode. *Electrocatalysis* **2017**, *8*, 366–374. [CrossRef]



© 2020 by the authors. Licensee MDPI, Basel, Switzerland. This article is an open access article distributed under the terms and conditions of the Creative Commons Attribution (CC BY) license (http://creativecommons.org/licenses/by/4.0/).